evaluate the intrinsic barriers for a properly chosen reaction series. Ingold and co-workers have reported the rate constants for reactions for $Et_3Si^•$ radicals with several organic halides.[11a] Figure 6 shows a graph of log k_T vs. the half-wave potenials of the halides. The curve through the data is drawn by using eq 11, with A = 0.5, B = 0.5, C = −57 kcal mol^{-1} (−2.5 V), and $\Delta G^‡(0)$ = 6.0 kcal mol^{-1}. Although the fit to the experimental results is not as good as that for the metal carbonyl radicals, it looks promising. It is noteworthy that the Arrhenius parameters (log A) vary in the order CCl_4, 10.2 ($E_{1/2}$ = −0.78 V); $C_6H_5CH_2Cl$, 8.9 ($E_{1/2}$ = −1.94 V); and CH_3Cl, 8.0 ($E_{1/2}$ = −2.76 V). The relationship suggests a tighter and more restricted transition state as the reaction becomes more endoergic, consistent with increased C–Cl bond rupture and Si–Cl bond formation.

Conclusions

The results reported here provide the first opportunity to test the applicability of the Marcus/Agmon–Levine equation, eq 8, or the Rehm–Weller equation, eq 12, with a significant body of experimental data for halogen atom transfer. For two reaction series involving rhenium carbonyl radicals the results are quite good. This suggests that the atom transfer processes under study conform to the assumptions of the model, most notably, that the intrinsic barrier for the reaction is comparatively constant as the halogen donor is varied. Second, the fact that log k_T correlates with the irreversible half-wave reduction potentials for the organic halides suggests that electron transfer plays a significant role in the reaction. The fit of the data to eq 11 suggests also that a single value of $\Delta G^‡(0)$ applies to reactions that range from strongly exoergic (−25 kcal mol^{-1}) to mildly endoergic (+5 kcal mol^{-1}).

Aside from the extent to which electron transfer is important in the atom transfer process, the fact that the data can be fitted by eq 11 is important. The basic assumptions regarding atom transfer processes embodied in eq 8 provide a useful basis on which to understand the effect of variations in both atom donor and metal carbonyl radical on the atom transfer rate constant. Further, eq 8 provides a means for relating the atom transfer reactions of the radicals to other, more obviously outer-sphere type electron transfer reactions of the radicals.[31]

(31) Rushman, P.; Brown, T. L. *J. Am. Chem. Soc.*, in press.

Photochemistry of $Fe(CO)_5$ Adsorbed onto Porous Vycor Glass

Michael S. Darsillo, Harry D. Gafney,*† and Michael S. Paquette*‡

Contribution from the Department of Chemistry, City University of New York, Queens College, Flushing, New York 11367, and Inorganic Materials and Catalyst Laboratory, Dow Chemical Company, Midland, Michigan 48420. *Received October 27, 1986*

Abstract: $Fe(CO)_5$ physisorbs onto porous Vycor glass without disruption of its primary coordination sphere. The spectral properties of the adsorbed complex mirror those found in fluid solution, and UV photolysis in vacuo leads to formation of the tetracarbonyl with a quantum yield of unity. The tetracarbonyl rapidly reacts with the PVG surface and chemisorbed water to form the spectrally distinct, oxidative addition products H–$Fe(CO)_4$–OSi and H–$Fe(CO)_4$–OH. These undergo secondary photolysis to form, depending on the initial loading, either elemental iron or the trimeric cluster $Fe_3(CO)_{12}$. Diffuse reflectance FTIR spectra, recorded after CW or pulsed laser excitation, establish the presence of dimeric and trimeric intermediates. Trapping experiments with CO and trimethylphosphine indicate a photochemically driven, stepwise reaction sequence in which the so-called "mobile intermediate", principally $Fe(CO)_3$, reacts with H–$Fe(CO)_4$–OH and $Fe(CO)_5$(ads) to form dimeric and trimeric products.

Hybrid catalysts composed of supported transition-metal carbonyls offer advantages of both homogeneous and heterogeneous catalysts.[1] Iron carbonyl, for example, has been examined on a number of supports[1] because of its catalytic activity in homogeneous solution.[2,3] Whether in solution or confined to a support, catalytic activity of the complex requires vacant or labile reaction sites where the substrate can bind and undergo chemical transformation.[4-6] In most cases, but particularly those involving hybrid systems, the complex is thermally activated.

$Fe(CO)_5$ physisorbs onto HY zeolite with a heat of adsorption of 2 kcal/mol.[7] Changes in the ^{13}C chemical shift and line width indicate that thermal decomposition of the complex, which occurs stepwise with an increasing, but weak interaction with the surface, leads to highly dispersed, atomic iron.[7] Adsorption of mono- and polynuclear iron carbonyls onto dehydrated HY zeolites, however, differs.[8] Adsorption of $Fe(CO)_5$ and $Fe_2(CO)_9$ occurs with the evolution of CO and results in identical adsorbate IR spectra, the latter being superimposed spectra of $Fe(CO)_5$ and $Fe(CO)_4Q$ where Q represents a lattice oxygen of the support.[8] Evacuation at 60 °C causes further CO evolution and formation of $Fe_3(CO)_{12}$.[8] Adsorption of $Fe_3(CO)_{12}$, on the other hand, occurs without CO evolution, and the IR spectrum of the adsorbed trimer is similar to that in fluid solution.[8] Nevertheless, changes in the spectrum of the zeolite and low-frequency shifts of the bridging ν_{CO} bands suggest the formation of a Lewis acid adduct where the bridging CO's interact with surface hydroxyls of the zeolite supercage. Thermal activation of the adsorbed trimer leads to decarbonylation. H_2 and CO_2 evolution, which occurs at 200 °C, is followed by CH_4 evolution at 250 °C.[8]

Thermal activation $Fe(CO)_5$ adsorbed onto Grafoil, a high surface area, oriented graphite support, causes CO evolution and formation of metallic iron preferentially at the edges or other dislocations in the graphite structure.[9] $Fe(CO)_5$ and $Fe_3(CO)_{12}$ reversibly adsorb onto hydroxylated silicas, whereas adsorption onto alumina, magnesia, and zinc oxide is irreversible due to

† City University of New York, Queen's College.
‡ Dow Chemical Company.

(1) Bailey, D. C.; Langer, S. H. *Chem. Rev.* **1981**, *81*, 109-148.
(2) Wender, I.; Pino, P. *Organic Synthesis Via Metal Carbonyls*; Interscience: New York, 1968.
(3) Taqui Khan, M. M.; Martell, A. E. *Homogeneous Catalysis in Metal Complexes*; Academic: New York, 1974; Vols. 1 and 2.
(4) Nakamura, A.; Tsutsui, M. *Principles and Applications of Homogeneous Catalysis*, Wiley: New York, 1980; pp 24-25.
(5) Parshall, G. W. *Homogeneous Catalysis*; Wiley: New York, 1980; pp 5-21.
(6) Slocum, D. W.; Hughes, O. R. *Ann. N.Y. Acad. Sci.* **1980**, *53*.
(7) Nagy, N. B.; Eenoo, M. V.; Derouane, E. G. *J. Catal.* **1979**, *58*, 230-7.
(8) Ballivet-Tkatchenko, D.; Coudurier, G. *Inorg. Chem.* **1979**, *18*, 558-64.
(9) Phillips, J.; Clausen, B.; Dumesic, J. A. *J. Phys. Chem.* **1980**, *84*, 1814-22.

0002-7863/87/1509-3275$01.50/0

formation of the hydrido cluster $[HFe_3(CO)_{11}]^-$.[10] Thermal decomposition on these supports depends on the water content of the support. On dehydroxylated MgO and Al_2O_3, thermal decomposition at 373 K under vacuum does not result in H_2 evolution and leads to FMR resonances consistent with zerovalent iron.[10] On the hydroxylated supports, adsorption yields the hydrido complex and thermal decomposition leads to H_2 evolution and FMR resonances indicative of zerovalent and oxidized iron.[10] Temperature-programmed decomposition of $Fe(CO)_5$ adsorbed on alumina evolves 3 mol of CO/mol of complex and suggests that the subcarbonyl species $Fe(CO)_2$, the dominant decomposition product at 373 K, is stabilized by the support.[11] In general, thermal activation of adsorbed iron carbonyls leads to CO dissociation and, depending on the hydration of the support, formation of highly dispersed, zerovalent or oxidized iron.

Transition-metal carbonyls, particularly iron carbonyls, possess a rich photochemistry, and photoactivation of a surface confined complex is an alternative route to catalytically active species.[12] Although recent experiments in this and other laboratories indicate that the primary process of adsorbed metal carbonyls is equivalent to that in fluid solution,[13-16] the secondary chemistry can be quite different.[17,18] Coordination to a surface functionality can stabilize the primary photoproduct, influence its surface mobility, and change its optical absorption characteristics.[13] Each or some combination of these changes modifies the secondary photochemical reactions. Consequently, photoactivation of an adsorbed metal carbonyl may lead to different behavior from that observed in fluid solution and, since photoactivation is generally at room temperature, from that observed in the thermal activation of the adsorbed complex.

Jackson and Thrushiem report that UV photolysis of $Fe(CO)_5$ adsorbed onto silica gel leads to formation of the trimer $Fe_3(CO)_{12}$ even at considerably less than monolayer coverage.[18] This contrasts with the photochemical behavior of $Fe(CO)_5$ in the gas phase and liquid phase and in noncoordinating solvents where the dominant photoproduct is the dinuclear $Fe_2(CO)_9$ cluster.[19-22] Since $Fe_3(CO)_{12}$ formation occurs in solutions containing weak ligands,[23,24] a rationale for the change in reaction product is the participation of surface silanol and siloxane groups in the reaction sequence.[18,25]

In addition to the chemical nature of the support surface, recent work has emphasized the role of surface dimensionality in the reactions of surface-confined species.[26] The surfaces of many currently used supports are not characterized by regular, translationally invariant lattices.[26-28] Rather, these highly irregular surfaces possess a dilatation symmetry and are characterized by a fractal or Hausdorff dimension.[28] The latter, which can be less than the dimensionality accessible to a molecule in the gas phase or in fluid solution, can impose further constraints on the reactivity of a surface-confined molecule. In fact, geometric factors may outweigh chemical factors in determining the kinematics of surface-confined molecules.[26]

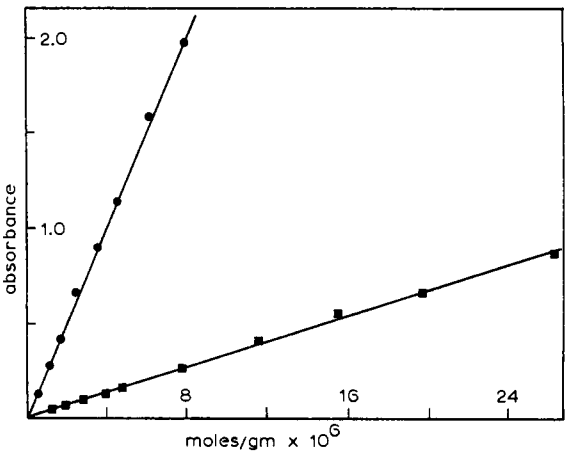

Figure 1. Optical density of $Fe(CO)_5$(ads) at 350 (●) and 400 nm (■) as a function of the moles of complex adsorbed/g of PVG.

Characterizing the photochemistry of adsorbed metal carbonyls is, in our opinion, essential to their potential use as catalysts. Yet such experiments are difficult, the difficulty being the opacity of the support.[18] Jackson and Thrusheim circumvented this difficulty by a clever use of a transparent silica gel. Our approach is to use Corning's code 7930 porous Vycor glass, PVG, as a support. PVG is a transparent, surface-hydroxylated silica, which contains a myriad of randomly dispersed, interconnected 70 ± 21 Å diameter pores. The similarities and differences between silica gel and PVG have been described.[29-31] Chemically, both possess hydroxylated surfaces, yet recent measurements suggest that the dimensionalities of the supports may be quite different.[28,32]

In this paper, we describe the photochemical reactions of $Fe(CO)_5$ adsorbed onto PVG. UV-visible and diffuse reflectance FTIR (DRIFT) spectra establish that $Fe(CO)_5$ physisorbs onto PVG without disruption or significant distortion of its primary coordination sphere. Spectroscopic evidence, recorded after pulsed excitation with a UV laser, indicates the immediate formation of two spectroscopically distinct $Fe(CO)_4$ oxidative addition products. Continued photolysis leads to further decarbonylation and, depending on the initial loading, either zerovalent iron or the formation of dimeric and trimeric clusters. Intermediates, identified spectroscopically and by chemical trapping, are described, and the cluster products are shown to arise from secondary reactions of more highly unsaturated, mobile intermediates with $Fe(CO)_5$ and the more reactive $Fe(CO)_4$ oxidative addition product. A model of the photochemical behavior of the adsorbed complex, designated $Fe(CO)_5$(ads), is proposed in which the so-called "mobile intermediate" leading to cluster formation is principally $Fe(CO)_3$.

Experimental Section

Materials. $Fe(CO)_5$ (Pressure Chemical Co.) was vacuum distilled and stored in a freezer under an inert atmosphere. Absorption and IR spectra of the distilled complex were in excellent agreement with published spectra.[33-36] $Fe_2(CO)_9$ and $Fe_3(CO)_{12}$ (Pressure Chemical Co.) were used as received since their absorption and IR spectra were in excellent agreement with published spectra.[37-39] Trimethylphosphine

(10) Hugues, F.; Basset, J. M.; Taarit, Y. B.; Choplin, A.; Primet, M.; Rojas, D.; Smith, A. K. *J. Am. Chem. Soc.* **1982**, *104*, 7020-4.
(11) Brenner, A.; Hucul, D. A. *Inorg. Chem.* **1979**, *18*, 2836-40.
(12) Wrighton, M. S. *Chem. Rev.* **1974**, *74*, 401-30.
(13) Simon, R.; Gafney, H. D.; Morse, D. L. *Inorg. Chem.* **1983**, *22*, 573-4.
(14) Simon, R.; Gafney, H. D.; Morse, D. L. *Inorg. Chem.* **1985**, *24*, 2565-70.
(15) Doi, Y.; Yano, K. *Inorg. Chim. Acta* **1976**, *76*, L71-3.
(16) Liu, D. K.; Wrighton, M. S. *J. Am. Chem. Soc.* **1982**, *104*, 898-901.
(17) Dieter, T.; Gafney, H. D., submitted for publication in *J. Am. Chem. Soc.*
(18) Jackson, R. L.; Trusheim, M. R. *J. Am. Chem. Soc.* **1982**, *104*, 6590-6.
(19) Graham, W. A. G.; Jetz, W. *Inorg. Chem.* **1971**, *10*, 4-9.
(20) Chisolm, M. H.; Massey, A. G.; Thompson, N. R. *Nature (London)* **1966**, *211*, 67.
(21) Dewar, J.; Jones, H. O. *Proc. R. Soc. London, Ser. A* **1905**, *76*, 558.
(22) Braye, E. H.; Huebel, W. *Inorg. Synth.* **1966**, *8*, 178.
(23) Schubert, E. H.; Sheline, R. K. *Inorg. Chem.* **1966**, *5*, 1071-4.
(24) Koerner Von Gustorf, H.; Dipetro, C. *Z. Naturforsch., B: Anorg. Chem., Org. Chem.* **1966**, *B21*, 42-5.
(25) Jackson, R. L.; Trusheim, M. R. *J. Phys. Chem.* **1983**, *87*, 1910-6.
(26) Pfiefer, P.; Avnir, D. *J. Chem. Phys.* **1983**, *79*, 3558-65.
(27) Avnir, D.; Farin, D.; Pfiefer, P. *J. Chem. Phys.* **1983**, *79*, 3566-71.
(28) Avnir, D.; Farin, D.; Pfiefer, P. *Nature (London)* **1984**, *308*, 261-3.
(29) Iler, R. K. *The Chemistry of Silica*; Wiley-Interscience: New York, 1979; p 551.
(30) Hair, M. L.; Chapman, I. D. *J. Am. Ceram. Soc.* **1966**, *49*, 651; *Trans. Faraday Soc.* **1965**, *61*, 1507.
(31) Cant, N. W.; Little, L. H. *Can. J. Chem.* **1964**, *42*, 802-9; **1965**, *43*, 1252-4.
(32) Evan, U.; Rademan, K.; Jortner, J.; Manor, M.; Reisfeld, R. *Phys. Rev. Lett.* **1984**, *52*, 2164-7.
(33) Lundquist, R. T.; Cais, M. *J. Org. Chem.* **1962**, *27*, 1167-72.
(34) Dartiguenave, M.; Dartiguenave, Y.; Gray, H. B. *Bull. Soc. Chim. Fr.* **1969**, *12*, 4223-5.
(35) Sheline, R. K.; Pitzer, K. S. *J. Am. Chem. Soc.* **1950**, *72*, 1107-12.
(36) Cataliotti, R.; Foffani, A.; Marchetti, L. *Inorg. Chem.* **1971**, *10*, 1594-7.

(Strem) and carbon monoxide (Linde or Matheson, CP grade) were also used as received since the reported purities were ≥99%. Spectral grade solvents were distilled over CaH_2 and stored over molecular sieves prior to use.

Code 7930 porous Vycor glass containing 70 ± 21 Å diameter cavities was obtained from the Corning Glass Works. Pieces (25 mm × 19 mm × 4 mm) of PVG were continuously extracted with distilled water for 24 h and then dried at 60 °C under reduced pressure ($p \leq 10^{-4}$ torr). The dried samples were calcined in air at 550 °C for at least 24 h and stored at this temperature until needed. For diffuse reflectance FTIR (DRIFT) experiments, extracted, dried pieces of PVG were crushed to a 325-mesh powder (≤45 μm). The powder was calcined at 550 °C for 12 h and then transferred while hot to tightly capped vials which were stored in an oxygen- and water-free glovebox.

Impregnation Procedures. Impregnation with $Fe(CO)_5$ was by vapor deposition where the moles adsorbed was determined by differential pressure measurements.[40] Weighed, calcined pieces of PVG were weighed and mounted upright in a Pyrex vacuum line equipped with MKS Baratron Models 315, BHS-1000, and 315 BHS-1 capacitance pressure sensors and a MKS Baratron Model 170 monitor. The line was evacuated to a pressure of $\leq 10^{-6}$ torr, and distilled $Fe(CO)_5$, which had been degassed by three freeze–pump–thaw cycles, was admitted to the line. Equilibration occurred in a matter of minutes, and the pressure drop was recorded. Identical measurements were performed without the PVG sample to correct for adsorption onto other surfaces, and the moles of $Fe(CO)_5$ adsorbed onto the PVG sample were calculated from the corrected pressure drop. Samples containing from 2.0×10^{-8} to 2.0×10^{-5} mol of $Fe(CO)_5$(ads)/g of PVG were prepared in this manner. Since absorption spectra recorded at different locations on the same sample established a uniform distribution of the complex on the PVG surface, a calibration plot (Figure 1) of $Fe(CO)_5$(ads) optical density at 350 and 400 nm vs. the mol of complex adsorbed/g of PVG was constructed. The moles of complex adsorbed onto subsequent samples, which ranged from 10^{-7} to 10^{-4} mol of $Fe(CO)_5$(ads)/g of PVG, were determined from this plot and their optical density.

Calcined pieces of PVG were transferred while hot to a previously described rectangular quartz cell.[14,17] The cell was attached to the vacuum line and evacuated ($p \leq 10^{-4}$ torr) while the sample cooled to room temperature, 22 ± 1 °C. The sample was exposed to degassed $Fe(CO)_5$, allowed to equilibrated, and then reevacuated to remove $Fe(CO)_5$ remaining in the vapor phase. Tests with the empty cell showed that adsorption onto the cell walls was spectrally undetectable, and the moles of complex adsorbed onto PVG was determined from its optical density and the above calibration plot. Because of an inherent spectroscopic uncertainty of ≤8%, due to light scattering by the random internal pore structure of PVG,[41] however, there is an uncertainty of ca. 10% in the moles adsorbed determined by this spectroscopic technique.

Impregnation with $Fe_2(CO)_9$, because of the low solubility of the complex, was by sublimation or mixing the complex with the powdered glass. Impregnation with $Fe_3(CO)_{12}$ was by previously described solution or sublimination techniques.[17] Weighed, calcined pieces of PVG were immersed upright in degassed, 10^{-3} M *n*-hexane solutions of $Fe_3(CO)_{12}$. The absorbance of the solution phase was monitored during adsorption, and the moles of complex adsorbed was calculated from the absorbance change at 605 nm. After being soaked, the samples were rigidly mounted in the rectangular quartz cell, and the solvent incorporated during impregnation was removed under vacuum. In the sublimation technique, a piece or powdered sample of PVG was suspended above the solid complex, the chamber was evacuated, and the complex was sublimed onto the support under vacuum at 60 °C. Absorption spectra recorded at different locations on the same sample established that impregnation by solution or sublimation techniques led to a uniform distribution of the complex on the PVG surface.

Neither technique nor those used to impregnate pieces of PVG with $Fe(CO)_5$, however, led to a uniform cross-sectional distribution. Previously described grinding procedures[42] and breaking freshly impregnated samples showed that, regardless of the moles of adsorbed, the complexes penetrated 0.4 ± 0.1 mm into the PVG sample. Thus, the samples examined in these experiments are surface-impregnated where the adsorbed complexes are limited to volumes of PVG adjacent to the outer surfaces.

Photolysis Procedures. Samples of PVG impregnated with $Fe(CO)_5$(ads) were irradiated in a Rayonet photochemical reactor (Southern New England Ultraviolet Co.) equipped with either 350-, 310-, or 254-nm bulbs. Quantum yield measurements, however, were limited to 350-nm excitation since competitive absorption by PVG is negligible at this wavelength. The excitation intensity was determined by ferrioxalate actinometry[43] and was typically 2×10^{-9} einsteins/(s cm^2).

In the time resolved experiments, diffuse reflectance FTIR (DRIFT) spectra of the adsorbate were recorded on a Nicolet Model 60SX FTIR equipped with a narrow-band MCT detector. A diffuse reflectance beam condensor (Harrick Scientific Model DRA-PMN) mounted in the sample compartment was modified to accept a custom designed diffuse reflectance microreactor. The microreactor, which has a 26 mm × 3 mm × 2 mm sample bed, was loaded with calcined, 325-mesh PVG in a dry, inert-atmosphere box. A BaF_2 window, which is transparent to UV, visible, and infrared radiation, was attached above and in contact with the 325-mesh sample. This arrangement, i.e., contact between the sample and the BaF_2 window, allowed the recording of adsorbate spectra without interference from reagents in the gas phase. The microreactor was then mounted on a translational stage that allowed 3-mm diameter spots to be sampled along the entire 26-mm length of the sample bed. The sample compartment of the spectrometer was modified to pass electrical, gas flow, vacuum, liquid flow, and auxiliary purge lines to the microreactor as well as a shaft for positioning the translational stage. Quartz windows were installed in the spectrophotometer sample compartment cover to admit the exciting radiation. These windows were masked during all manipulations to prevent photochemistry prior to the experiment.

The lines attached to the microreactor were connected to a vacuum system consisting of a forepump (Edwards Model E2M5), diffusion pump (Edwards Model E01), trap, metal lines, and fittings (Cajon Ultratorr), bellows sealed valve (Nupro), and capacitance pressure sensors (MKS Baratron Models 315BHS-1000 and 315 BHS-1) and monitors. An auxiliary gas manifold equipped with needle valves and a Penning sensor (Edwards Model CP25) and controller (Edwards Model 8) was used to evacuate the microreactor to a pressure of 2×10^{-6} torr. Gas samples were then prepared in this line (total volume 102 mL) and were admitted to the microreactor cell in the FTIR sample compartment through narrow bore tubing (total volume 1.5 mL). The powdered PVG was impregnated with $Fe(CO)_5$ by expanding a set quantity, generally 5 torr in 102 mL, into the microreactor cell. After equilibration, the cell was closed off and the loading was calculated to be 3×10^{-4} mol of $Fe(CO)_5$/g of PVG. The manifold was then reevacuated, other gases such as CO and $P(CH_3)_3$ were admitted to the reactor, and the desired equilibrium pressure was established.

In a typical DRIFT experiment, background spectra, i.e., spectra of the unimpregnated PVG in the evacuated microreactor, were recorded in each sampling position. $Fe(CO)_5$ was expanded into the cell, and after equilibration initial spectra were recorded at the sampling position. In a trapping experiment, the impregnated sample was then exposed to various CO or $P(CH_3)_3$ pressures. The samples were irradiated at 350 nm with a Kr ion laser (Coherent Model CR3000K) or at 355 nm with the second harmonic from a Q-switched Nd:YAG laser (Quanta Ray Model DCR-2). The Kr ion laser intensity was adjusted to provide 500 mW to an area, 0.13 cm^2, slightly larger than FTIR sampling area. The exposure time was controlled with an electronic shutter (Newport Research Model 880) timed to open between the spectrophotometer data acquisition periods. The Nd:YAG laser provided 50 mJ (40 mW/cm^2) of Q-switched 355-nm radiation to the same sample area. The laser flashlamps were synchronized with the spectrometer data acquisition rate, and the Q-switch was fired between the spectrometer scans. In most cases, a second program was initiated immediately after excitation which acquired spectra over a longer time interval. After completion of the data acquisition for a given set of experiments, the interferograms were transformed, co-added, and ratioed against the appropriate background. The reflectance spectra were then converted to Kubelka Munk spectra for evaluation. For different exposure times or pulse configurations, the sample was moved to a new position with the translational mount where it was spectroscopically verified that no chemistry had occurred.

Physical Measurements. Gaseous photoproducts were collected with a Toepler pump and analyzed with a Gow Mac Model 100 gas chromatograph equipped with a 6 ft × 1/4 in. column containing 5-Å molecular sieve (Supelco) packing and a Re–W thermal conductivity detector. The column was maintained at 100 °C, and He was used as the carrier gas (40 mL/min) to quantitate CO evolution whereas Ar was used as the carrier gas to quantitate CO and H_2 evolution. The detector response, calibrated with aliquots of each gas, was displayed on a Shimazadu Model R111 recorder. UV–visible spectra were recorded on a

(37) Gray, H. B.; Levenson, R. A.; Tyler, D. B. *J. Am. Chem. Soc.* **1978**, *100*, 7888–93.
(38) Turner, J. J.; Poliakoff, M. *J. Chem. Soc. D* **1970**, 1008–9.
(39) Mays, M. J.; Knight, J. *J. Chem. Soc. D* **1970**, 1006–7.
(40) Ross, S.; Olivier, J. P. *On Physical Adsorption*; Wiley-Interscience: New York, 1964; p 31.
(41) Kennelly, T.; Gafney, H. D.; Braun, M. *J. Am. Chem. Soc.* **1985**, *107*, 4431–40.
(42) Wolfgang, S.; Gafney, H. D. *J. Phys. Chem.* **1983**, *87*, 5395–401.
(43) Calvert, J. G.; Pitts, J. N. *Photochemistry*; Wiley: New York, 1971; pp 780–8.

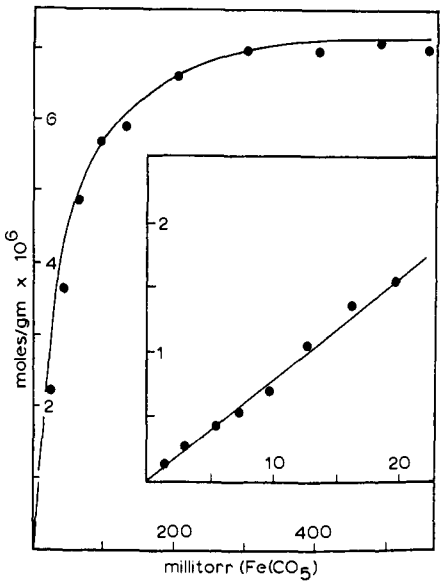

Figure 2. Adsorption isotherm of $Fe(CO)_5$ on PVG plates at 26 °C.

Cary 14 spectrophotometer modified to hold the rectangular cells. FMR spectra of products generated on coarsely crushed PVG were recorded at room temperature, 22 ± 1 °C, on an IBM-Bruker Model ER200E-SCR spectrometer. No resonance was detected from the unimpregnated PVG. Infrared spectra of solutions or mulls were recorded on a Perkin-Elmer Model 1330 spectrophotometer, calibrated against polystyrene, and equipped with a Model 1600 data station.

Results

Adsorption of $Fe(CO)_5$(ads). Thermal gravimetric analysis of PVG indicates the presence of both bulk and chemisorbed water. Bulk water desorbs at 100–120 °C while chemisorbed water desorbs slowly up to the onset of consolidation, ca. 700 °C. DRIFT spectra recorded under flowing He as a function of temperature show that the intense, broad absorption due to water, centered at 3500 cm^{-1} declines, and at 550 °C the spectrum exhibits a sharp, intense band at 3744 cm^{-1} with a shoulder at 3655 cm^{-1} which have been assigned to free and hydrogen-bonded silanol groups, respectively.[30,31] However, a weak band due to small amounts of chemisorbed water remains. The intensity of this band varys from sample to sample but after calcination is always ≤10% of that of the 3744 cm^{-1} silanol band.

Adsorption of $Fe(CO)_5$ onto PVG is a linear function of pressure over the range 0.125–2.04 torr, and the isotherm measured at 26 °C (Figure 2) resembles that reported for adsorption of the complex onto silica gel.[18] UV–visible spectra recorded at different locations on an impregnated sample are within experimental error, which establishes a uniform distribution of the complex on the PVG surface. Regardless of the moles of $Fe(CO)_5$ adsorbed, however, the complex does not penetrate throughout the entire pore volume. Breaking samples containing 2×10^{-5} mol/g shows that $Fe(CO)_5$ penetrates 0.4 ± 0.1 mm into PVG and, as found with other complexes,[17,42] impregnates volumes of PVG adjacent to the outer geometric surfaces of the sample. Since the adsorbate is not uniformly distributed throughout the entire pore volume, surface coverage cannot be uniquely defined. Rather, a lower limit is calculated where it is assumed that the surface area within the impregnated volumes, 130 m^2/g of PVG,[41] corresponds to that measured by N_2 adsorption at low temperature. Taking the area occupied by $Fe(CO)_5$(ads) to be 0.3 nm^2, the samples prepared in these experiments, which range from $\leq 10^{-7}$ to 3×10^{-4} mol of $Fe(CO)_5$/g of PVG, correspond to fractional surface coverages of ≤0.15%–45%. The calculated values are approximations, however, and are used in a relative rather than absolute sense.

Adsorption of $Fe(CO)_5$ onto PVG is reversible, although the rates of desorption from plate and powdered samples differ. IR bands of $Fe(CO)_5$ adsorbed on powdered PVG, 3×10^{-4} mol/g, disappear within 5 min at room temperature when the DRIFT microreactor is evacuated, whereas desorption from plate samples

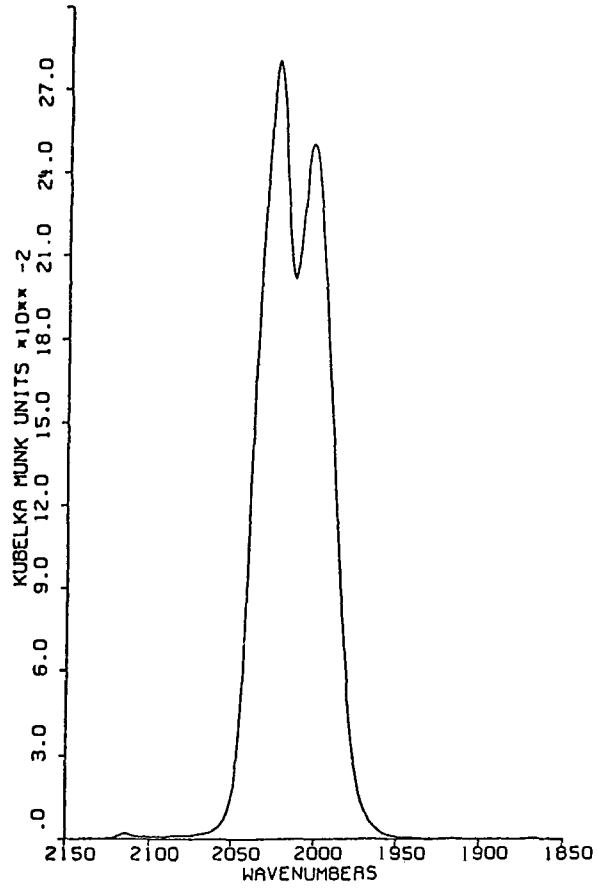

Figure 3. Diffuse reflectance FTIR spectrum, plotted in Kubelka–Munk absorbance units, of $Fe(CO)_5$ physisorbed onto PVG.

is considerably slower. Evacuation of a quartz cell containing a 25 mm × 25 mm × 4 mm sample impregnated with (4.0 ± 0.4) × 10^{-6} mol of $Fe(CO)_5$/g causes a steady decline in the UV spectrum, but optical density attributable to the adsorbed complex is discernible after several hours. The difference in desorption rates is thought to reflect differences in penetration depth; i.e., adsorption onto powdered PVG, because of its larger outer surface area, is principally limited to the outer surfaces of the particles whereas adsorption onto the plate samples, as described above, leads to limited impregnation of interior pores.

Spectroscopic Properties of $Fe(CO)_5$(ads). The electronic spectrum of $Fe(CO)_5$(ads) consists of a strong, featureless absorption in the UV associated with MLCT and ligand-localized transitions. The spectrum resembles that of the complex in fluid solution except that lower energy ligand field transitions, which appear as shoulders at 245 and 285 nm in the fluid solution spectrum, are not discernible.[33,34] The DRIFT spectrum of the adsorbed complex (Figure 3) exhibits intense bands at 2004 and 2026 cm^{-1} and a weak band at 2114 cm^{-1}. Relative to the IR spectrum of $Fe(CO)_5$ in the vapor phase where the major CO bands occur at 2012 and 2033 cm^{-1}, these bands are red-shifted and their relative intensities are inverted. The weak band at 2114 cm^{-1}, which is not observed in the vapor- or solution-phase spectra of the complex, is assigned to the symmetric ν_1 mode.[44] The latter occurs at 2116 cm^{-1} in the Raman spectrum of liquid $Fe(CO)_5$ and appears as a weak band at 2115 cm^{-1} in the IR spectrum of crystalline $Fe(CO)_5$ due to a C_2 site symmetry.[36] Bein and Jacobs also assign weak bands in the 2115 cm^{-1} region of the spectrum of $Fe(CO)_5$ adsorbed onto zeolites to the ν_1 mode and suggest that perturbations imposed by the adsorbent reduces the molecular symmetry of the adsorbate.[45] The appearance of the ν_1 mode, albeit weak, suggests that some distortion occurs when $Fe(CO)_5$

(44) Bigorgne, M. *Organomet. Chem.* **1970**, *24*, 211.
(45) Bein, T.; Jacobs, P. A. *J. Chem. Soc., Faraday Trans.* **1983**, *79*, 1819–31.

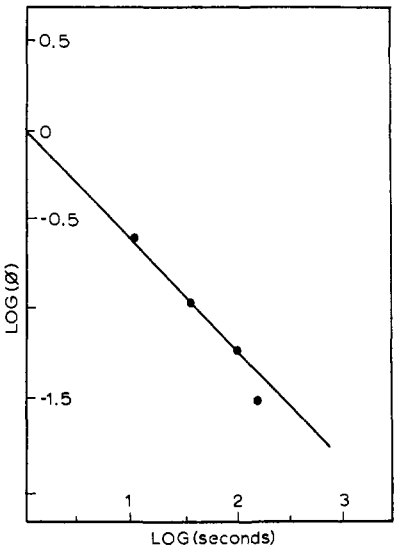

Figure 4. Quantum yield of $Fe(CO)_5$ disappearance vs. photolysis time during 350-nm photolysis of a sample containing 10^{-6} mol of $Fe(CO)_5$(ads)/g in vacuo at 22 ± 1 °C.

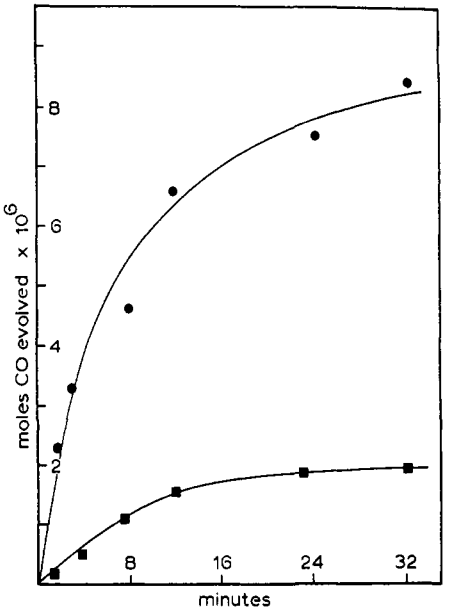

Figure 5. Moles of CO evolved (●) during a 350-nm photolysis of 10^{-5} mol of $Fe(CO)_5$(ads)/g. Theoretical yield of CO (■) assuming 3 mol of CO/mol of $Fe_3(CO)_{12}$(ads) formed.

is adsorbed on PVG. This distortion may also account for the change in the relative intensities of the intense asymmetric CO bands. In spite of the distortion, the similarity of the vibrational and electronic spectra of the adsorbed complex with vapor- and solution-phase spectra, particularly the absence of lower energy ligand field transitions indicative of ligand substitution, as well as the ability to desorb the intact complex establishes that the complex physisorbs onto PVG without significant molecular change.

Photochemical Reactions of $Fe(CO)_5$(ads). Unlike that observed on silica gel where $Fe_3(CO)_{12}$ is the dominant product at 25 °C regardless of the initial loading,[18] the photochemistry of $Fe(CO)_5$(ads) on PVG exhibits a pronounced dependence on loading. Photolysis of samples containing $\leq 10^{-6}$ mol/g in vacuo at 22 ± 1 °C with 350-, 310-, or 254-nm light causes a decline in the UV characteristic of $Fe(CO)_5$(ads) and a concurrent growth of a broad absorption centered at 370 nm. An isosbestic point at 285 nm is maintained during short irradiation times, and exposure to 1 atm of CO regenerates the $Fe(CO)_5$(ads) spectrum in ≥97% yield. The similarity of the photoproduct spectrum with that of $Fe(CO)_4$ generated in low-temperature matrices[46] indicates that the primary photoreaction is

$$Fe(CO)_5(ads) \rightarrow Fe(CO)_4(ads) + CO \qquad (1)$$

The absence of a near-IR absorption characteristic of free $Fe(CO)_4$,[47,48] however, suggests that the vacant coordination site of the surface-bound tetracarbonyl $Fe(CO)_4$(ads) is occupied by either a silanol group or chemisorbed water. We will return to the characterization of the initial photoproduct below. It should be realized that although designated $Fe(CO)_4$(ads), in fact, the absence of a near-IR absorption points to a surface-bound tetracarbonyl.

Reaction 1 is independent of excitation wavelength, i.e., 350, 310, and 254 nm. However, quantum yield measurements are limited to 350 nm where competitive absorption by the support is negligible. As shown in Figure 4, plots of ϕ_{obsd} vs. irradiation time extrapolate to a limiting yield, 0.96 ± 0.05, within experimental error of unity. This high efficiency is an experimental difficulty since the product forms rapidly and undergoes secondary photolysis with a similar high efficiency.

Continued photolysis of samples containing $\leq 10^{-6}$ mol of $Fe(CO)_5$(ads)/g, particularly with 300- or 254-nm light, leads to the evolution of 4.9 ± 0.2 mol of CO/mol of $Fe(CO)_5$(ads). UV–visible spectra recorded during photolysis, however, do not reveal absorptions assignable to distinct monomeric or polymeric iron carbonyls. At 280 nm, for example, the relative absorptivity of $Fe_3(CO)_{12}$ is 4.8 times that of $Fe(CO)_5$ both in solution and adsorbed onto PVG.[49] Yet, a continual decline in absorbance at 280 nm as well as no detectable absorbance at 605 nm indicates that $\leq 5 \times 10^{-6}$ mol of $Fe_3(CO)_{12}$ are formed/mol of $Fe(CO)_5$ reacted. With respect to the possible formation of $Fe_2(CO)_9$, similar results occur. $Fe_2(CO)_9$ powder dispersed in Florolube exhibits an intense absorption in the UV with a distinct shoulder centered at 440 nm. During photolysis of $Fe(CO)_5$(ads), no increase in absorption occurs at 440 nm which could be attributed to $Fe_2(CO)_9$ formation. In each experiment with samples containing $\leq 10^{-6}$ mol/g, the spectral changes consist of a general decline throughout the UV region. H_2 evolution, indicative of metal oxidation,[50,51] is not detected, ≤0.02 mol of H_2/mol of $Fe(CO)_5$ads, and exposing the photoproduct to 1 atm of CO at room temperature regenerates the absorbance at 370 nm assigned to surface-bound $Fe(CO)_4$(ads).[46-48] The latter change occurs within minutes and is followed by a slower reaction leading to $Fe(CO)_5$(ads).

In a number of experiments, the final photoproduct spectrum after extensive 254-nm photolysis consisted of a series of sharp bands superimposed on a rising UV background. The band spectrum is within experimental error of the spectrum of atomic iron generated in 20 K CH_4 matrices.[52] FMR spectra of the photoproduct at room temperature show a resonance with g = 2.070 and a line width of (5 ± 0.5) × 10^3 G. The FMR spectra are consistent with the formation of small iron particles[53] while the electronic spectra indicate the formation of some atomic iron. It must be emphasized, however, that the spectral results are not reproducible from sample to sample. Although GC analyses of the vapor-phase consistently indicated the evolution of 4.9 ± 0.2 mol of CO/mol of $Fe(CO)_5$(ads), in most experiments, the final

(46) Poliakoff, M.; Turner, J. J. *J. Chem. Soc., Dalton Trans.* **1973**, 1351–7.
(47) Poliakoff, M.; Turner, J. J. *J. Chem. Soc., Dalton Trans.* **1974**, 2276–85.
(48) Davies, B.; McNeish, A.; Poliakoff, M.; Turner, J. J. *J. Am. Chem. Soc.* **1979**, *99*, 7573–9.
(49) Wrighton, M. S.; Graff, J. L.; Reichel, C. L.; Sanner, R. D. *Transition Metal Mediated Organic Synthesis*; Slocum, D. W., Hughes, O. R., Eds.; New York Academy of Science: New York, 1980; Vol. 333, p 188.
(50) Brenner, A. *J. Chem. Soc., Chem. Commun.* **1979**, 251.
(51) Brenner, A.; Burwell, R. L. *J. Catal.* **1979**, *52*, 353–63.
(52) Poliakoff, M.; Turner, J. J. *J. Chem. Soc., Faraday Trans. 2* **1974**, *70*, 93–9.
(53) Hughes, F.; Bussiere, P.; Dalmon, J. A.; Basset, J. M.; Olivier, D.; Commereuc, D.; Chauvin, Y.; Bonneviot, L. Preprints, VII International Congress on Catalysis, Tokyo, 1980; paper A51.

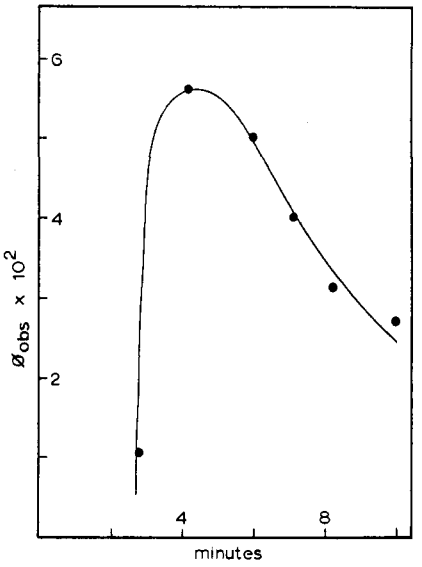

Figure 6. Quantum yield of $Fe_3(CO)_{12}$(ads) as a function of time during a 350-nm photolysis.

electronic spectrum consists of a nondescript, increasing absorbance in the UV region. Clearly, the level of aggregation of the decarbonylated iron varies from sample to sample. However, the photochemistry on PVG is consistent from sample to sample. At low loadings, UV photolysis of $Fe(CO)_5$(ads) in vacuo causes decarbonylation without concurrent oxidation of the metal and without spectral evidence of the formation of dimeric or trimeric intermediates.

Photolysis of PVG sample containing $\geq 10^{-6}$ mol of $Fe(CO)_5$(ads)/g in vacuo with 254-, 310-, or 350-nm radiation causes an immediate growth in absorption at 605 nm. The product spectrum agrees exactly with the visible spectrum of $Fe_3(CO)_{12}$(ads) and, like that found by Jackson and Thrusheim, establishes formation of $Fe_3(CO)_{12}$(ads). The stoichiometry of the reaction and the quantum yield of trimer formation, however, indicate a complex reaction sequence. GC analyses of the vapor phase (Figure 5) reveal considerably more CO than the theoretical yield assuming that 3 mol of CO are evolved/mol of $Fe_3(CO)_{12}$ formed; the latter determined by comparing the photogenerated absorbance at 605 nm with that of PVG samples containing known amounts of $Fe_3(CO)_{12}$(ads). The quantum yield of trimer formation, ϕ_T, shows a marked dependence on irradiation time. Samples containing from 3.7×10^{-6} to 2.5×10^{-5} mol of $Fe(CO)_5$/g exhibit an induction period (Figure 6) which suggests that formation of the trimer arises from secondary reaction(s) of the primary photoproduct. The electronic spectrum of $Fe_3(CO)_{12}$, both in solution[37] and adsorbed onto PVG, exhibits a band at 605 nm and a shoulder at 440 nm. Although the 605-nm band is immediately apparent, the 440-nm shoulder of the trimer could not be resolved in the photoproduct spectrum. Instead, a broad absorption centered at ca. 400 nm occurs, and comparison of the relative absorbances at 605 and 440 nm of the photolyzed sample with those of a known sample of $Fe_3(CO)_{12}$(ads) indicates the presence of additional photoproducts. Subtracting the absorbance attributable to $Fe_3(CO)_{12}$ in the 350–450-nm region, based on its absorbance at 605 nm, yields a spectrum with a maximum at 370–380 nm that closely resembles that of $Fe(CO)_4$(ads) (see above). Exposing the photoproduct to 1 atm of CO causes a rapid decline in absorbance in the near-UV while that at 605 nm remains unchanged. The absorption at 605 nm characteristic of the trimer does not appear when $Fe(CO)_5$(ads) is photolyzed under pressures of CO ranging from 400 torr to 1 atm. Photolysis develops a yellow color that quickly disappears in the time required to move the cell from the Rayonet reactor to the spectrophotometer. These results suggest that, regardless of initial loading, photolysis leads to surface-bound $Fe(CO)_4$(ads). At higher loadings, the latter undergoes further reactions leading to $Fe_3(CO)_{12}$(ads). However, there is no evidence in the electronic spectra recorded during photolysis of the formation of $Fe_2(CO)_9$.

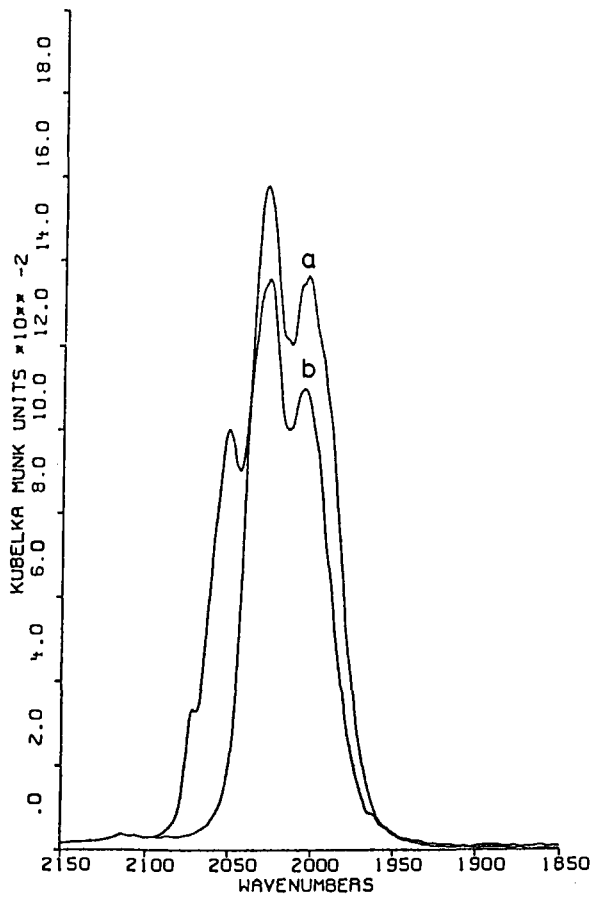

Figure 7. Kubelka–Munk spectra of $Fe(CO)_5$(ads) (a) before and (b) after single-pulse excitation (355-nm, 7-ns fwhm, 50 mJ, 40 mW/cm^2).

Diffuse Reflectance FTIR Experiments. Irradiation of powdered PVG containing 3×10^{-4} mol of $Fe(CO)_5$ads/g in vacuo with the 355-nm second harmonic of a Q switched Nd:YAG laser (50 mJ, 7-ns fwhm) causes significant loss of $Fe(CO)_5$ band intensity and, as shown in Figure 7, the appearance of two higher frequency bands at 2073 and 2048 cm^{-1}. The $Fe(CO)_5$ bands at 2026 and 2004 cm^{-1} return to their original intensity within 10 s after excitation. Since the latter change occurs without detectable change in the photoproduct band intensity, it is not due to a thermal back reaction. Rather, regrowth of the pentacarbonyl band intensity, which occurs in most experiments, is attributed to replenishment of the surface-depleted $Fe(CO)_5$ by diffusion through the powdered PVG in the microreactor. Consequently, $Fe(CO)_5$(ads) spectra are subtracted from spectra acquired at a later time to reveal minor features in the photoproduct spectra. Figure 8 illustrates difference spectra following two-pulse excitation of powdered PVG containing 3×10^{-4} mol of $Fe(CO)_5$/g in vacuo. The top spectrum is the difference between the initial $Fe(CO)_5$(ads) spectrum and that recorded immediately after excitation. The subsequent spectra are the difference between that recorded immediately after excitation and that recorded at the specified later times. Difference spectra highlight features that have decayed (positive bands) or grew in (negative bands) during the indicated time intervals. The first feature to decay is the high-frequency shoulder at 2073 cm^{-1}. Most of its decay occurs during the first 40 s after excitation and is accompanied by a loss of a shoulder at 2048 cm^{-1}. These bands are assigned to a single species since both decay at the same rate. A low-intensity band in the bridging carbonyl region, 1790 cm^{-1}, also appears and decays during this time interval. At longer times, i.e., $\geq$140 s, decay of the intense 2056 cm^{-1} band dominates the spectral change. This decay continues beyond the times shown in Figure 8, but at a slower rate. Similar results occur with single pulse excitation except that less product is formed, and the second

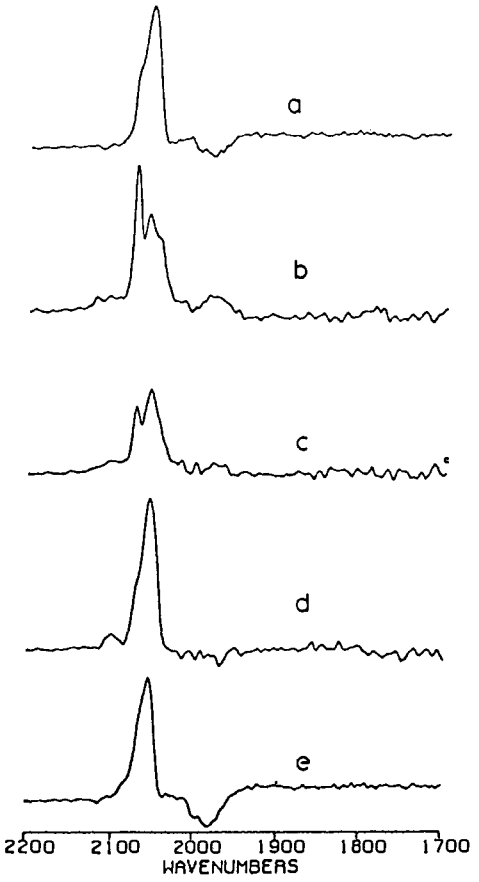

Figure 8. Difference spectra (see text) following two-pulse, 355-nm excitation (50 mJ/pulse) of $Fe(CO)_5$(ads) recorded (a) immediately, (b) 40 s, (c) 100 s, (d) 400 s, and (e) 540 s after excitation.

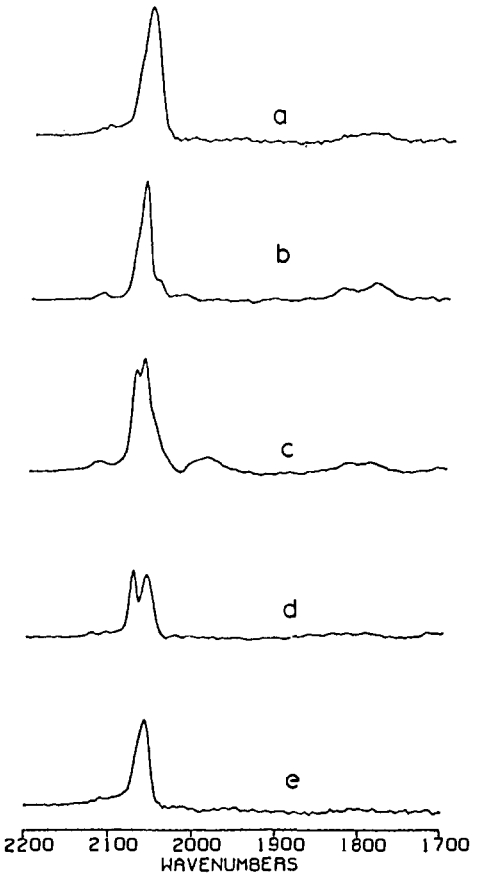

Figure 9. Difference spectra following a 0.1-s, 350-nm photolysis (500 mW/0.13 cm^2) of $Fe(CO)_5$(ads) recorded (a) immediately, (b) 100 s, (c) 200 s, (d) 400 s, and (e) 600 s after excitation.

pulse favors formation of the 2056 cm^{-1} absorption over an increase in the 2073 cm^{-1} absorption.

Bands in the 2053–2059 cm^{-1} region are indicative of a trimeric cluster, whereas bands in the bridging ν_{CO} region are indicative of dimeric adsorbates. The Kubelka–Munk spectrum of $Fe_3(CO)_{12}$(ads) displays a major absorption at 2053 cm^{-1} with a broad shoulder at 2032 cm^{-1} and a minor absorption at 2109 cm^{-1}; absorptions in the bridging ν_{CO} region are not detected. When dispersed in Fluorolube, $Fe_2(CO)_9$ displays broad bands at 2015 and 1820 cm^{-1}. If solid $Fe_2(CO)_9$ is mixed with powdered PVG, the spectrum of the mixture exhibits bands at 2051, 2028, 2005, and 1878 cm^{-1}. Since difference spectra reveal that much of the intensity of the 2028 and 2005 cm^{-1} bands is due to $Fe(CO)_5$ whereas the 2051 cm^{-1} absorption is due to $Fe_3(CO)_{12}$, the spectral change is attributed to disproportionation of $Fe_2(CO)_9$ that occurs on the PVG surface during mixing. Nevertheless, difference spectra reveal significant residual absorption remains under the $Fe(CO)_5$ bands. The bridging carbonyl band is of medium intensity and much broader than the terminal carbonyl absorptions. Although some similarity exists, the residual spectrum cannot be unambiguously assigned to $Fe_2(CO)_9$.

In contrast to pulsed excitation, which produces a grayish spot on impregnated PVG, CW excitation (350 nm, 500 mW) produces a pale green color similar to that observed when $Fe_3(CO)_{12}$ is formed on the plate samples. Difference spectra recorded after CW excitation reveal bands in the bridging ν_{CO} region as well as somewhat different absorptions in the terminal ν_{CO} region. In the bridging ν_{CO} region, the band intensities increase with increasing exposure time, which was varied from 0.1 to 1.6 s. The increase in band intensity, however, occurs without a change in their decay rates. The band intensities in the terminal ν_{CO} region exhibit a more complex time dependence. Figure 9 is representative of the spectral changes following 0.1 s excitation. Immediately after excitation, the spectrum after subtraction of absorptions due to $Fe(CO)_5$(ads) exhibits an intense absorption at 2059 cm^{-1} with a discernible high-frequency shoulder. During the first 100 s after excitation, a severe decline in the intensities of the bridging carbonyl absorptions at 1790 and 1820 cm^{-1} accompanies a loss in intensity at 2066 cm^{-1}. The intensities of these bands continue to decline during the next 100 s, and the decay of bands at 2073 and 2048 cm^{-1} becomes apparent. At later times, the bridging carbonyl absorptions and the band at 2066 cm^{-1} disappear and the 2073 and 2048 cm^{-1} bands dominate the decay. The latter decay to a spectrum exhibiting a single absorption at 2059 cm^{-1} which resembles that observed immediately after excitation.

In both CW and pulsed excitation experiments, the 2048 cm^{-1} band accompanies the appearance of the 2073 cm^{-1} band. The band intensities correlate well in the different experiments, and both bands decay at the same rate. Thus both bands are assigned to a single species whose decay characteristics suggest that it is an intermediate common to the formation and decay of other transients. For example, the rate of decay of the species responsible for the 2073 and 2048 cm^{-1} bands is much slower following CW excitation than it is following pulsed excitation. In addition, CW excitation produces a strong absorption at 2066 cm^{-1} that decays before the 2073–2048 cm^{-1} decay is apparent. This suggests that the species exhibiting the 2066 cm^{-1} band converts into the species displaying the 2073 and 2048 cm^{-1} bands, perhaps balancing its decay. Furthermore, spectra recorded at 80-ms intervals during 1.0-s CW excitation show that an early growth of a 2073 cm^{-1} is followed by a later growth of a strong 2063 cm^{-1} band. The latter comprises the quickly decaying 2066 cm^{-1} band and the slowly decaying 2058 cm^{-1} band.

Pulsed and CW excitation liberate CO during photolysis and consume it during the thermal back reactions. Consequently, experiments were performed under CO pressures ranging from 0.04 to 400 torr. Spectra recorded during 0.1-s irradiations (350 nm, 500 mW) under different CO pressures show that an initial formation of the 2073 and 2050 cm^{-1} bands is followed by the

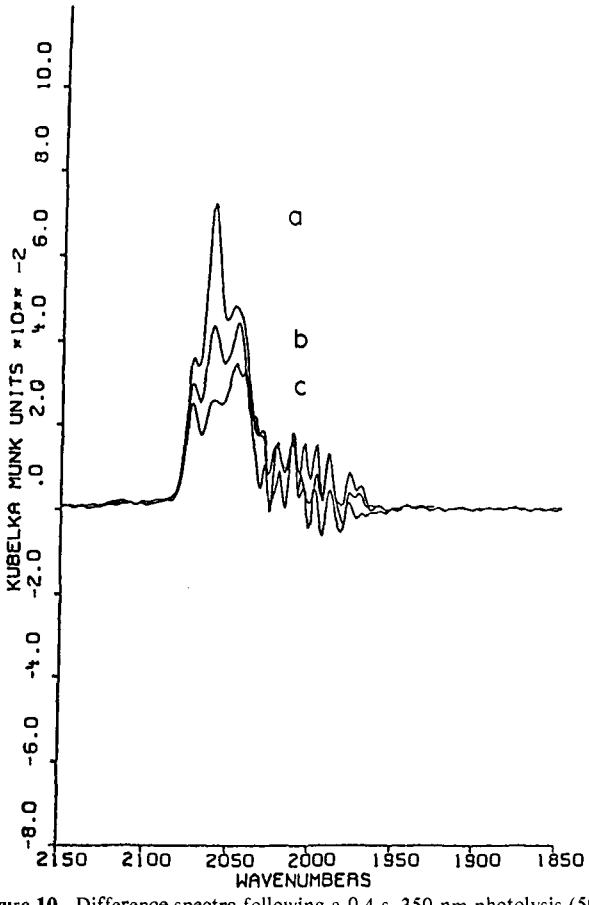

Figure 10. Difference spectra following a 0.4-s, 350-nm photolysis (500 mW/0.13 cm^2) of $Fe(CO)_5$(ads) under 400 torr of CO recorded (a) 0.8 s, (b) 1.5 s, and (c) 2.3 s after excitation.

rapid growth of the 2062 cm^{-1} band. Longer irradiation times and high CO pressures of 40 or 400 torr enhance the formation of the rapidly decaying 2062 cm^{-1} band. The order of product appearance and band maxima closely resemble that found in CO-free experiments (see above). In contrast to the CO-free experiments, however, where photoproduct decay occurs over hundreds of seconds (Figures 7 and 8), the presence of CO accelerates the thermal dark reactions. The relative rate of photoproduct decay increases by approximately an order of magnitude when the CO pressure is increased from 4 to 400 torr where photoproduct decay is essentially complete within 20 s following excitation. Figure 10 illustrates the spectral changes following 0.4-s excitation under 400 torr of CO. The 2062 cm^{-1} band disappears first followed by the decay of the 2073 and 2050 cm^{-1} bands. The rapid loss of the strong 2062 cm^{-1} absorption is not accompanied by an increase in the 2073 cm^{-1} absorption. The enhanced noise in the 2030–1980 cm^{-1} region is characteristic of strong Kubelka–Munk absorptions due to unreacted $Fe(CO)_5$(ads) and the fact that these are single scan spectra. At a CO pressure of 400 torr, however, the absence of a 2053 cm^{-1} band, characteristic of $Fe_3(CO)_{12}$(ads), indicates that CO intercepts the reactive precursors and prevents trimer formation. Similar band maxima occur under 4.0 torr of CO, but the band shapes differ and the rates of decays are considerably slower. The difference in band shape is due to the presence of a slowly decaying 2053 cm^{-1} band that, although occurring at slightly lower frequency, resembles the 2058 cm^{-1} band observed in CO-free experiments. Increasing the irradiation time at lower CO pressure leads to detectable bridging ν_{CO} absorptions at 1820 and 1790 cm^{-1}. Photolysis of $Fe(CO)_5$(ads) under 40 torr of CO yields results intermediate between those just described, whereas results under 0.4 or 0.04 torr of CO resemble CO-free experiments (see above).

Figure 11 illustrates the spectral changes following successive 350-nm irradiations of $Fe(CO)_5$(ads) under 100 torr of trimethylphosphine, TMP, which acts as an irreversible trap that

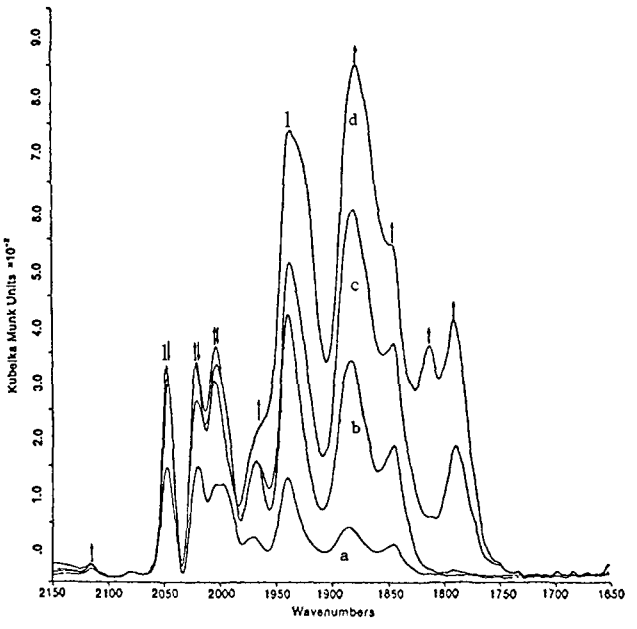

Figure 11. Difference spectra recorded following (a) 0.1-s, (b) 0.4-s, (c) 1.6-s, and (d) 6.4-s 350-nm photolyses (500 mW/0.13 cm^2) of $Fe(CO)_5$(ads) under 100 torr of $P(CH_3)_3$. Arrows indicate changes in band intensities with increasing irradiation time.

yields thermally stable phosphine-substituted photoproducts. As the photolysis proceeds, lower frequency bands at 1969, 1940, 1885, and 1846 cm^{-1} show a continuous increase in intensity whereas bands at higher frequencies exhibit a more complex dependence. During the first 0.4 s of irradiation, the bands at 2047, 2020, and 2004 cm^{-1} increase in intensity but then decline at longer irradiation times. The bands at 1814 and 1790 cm^{-1} are not present in the initial spectra. These bands appear at a later time, and the rate of increase in their intensity correlates with the decline in intensity of the higher frequency 2047, 2020, and 2004 cm^{-1} bands. Continued photolysis also causes changes in peak position and the shapes of several major bands. The difference between spectra recorded at later photolysis times shows that the change in band shape is due to the growth of absorptions at 1855, 1950, and 1920 cm^{-1} which develop during longer irradiation times.

As found in the other experiments, the photoinduced spectral changes under TMP undergo further change in the dark. Although spectra recorded after photolysis indicate a complex reaction sequence where several changes occur at once, these changes are minor perturbations, and spectra recorded at later times closely resemble those recorded immediately after excitation. However, photolysis in the presence of TMP leads to significant, irreversible consumption of the starting material since the $Fe(CO)_5$(ads) bands do not return to their original intensity.

Discussion

The surface of calcined PVG consists of free and hydrogen-bonded silanols, as well as small, but variable amounts of hydrogen-bonded water. Adsorption on to this surface either from solution or by vapor deposition does not lead to a uniform, cross sectional distribution. Regardless of the moles of $Fe(CO)_5$ adsorbed onto 25 mm × 25 mm × 4 mm plates of this porous support, which ranged from 2×10^{-8} to 2×10^{-5} mol/g, the complex penetrates 0.5 ± 0.1 mm into the sample and impregnates volumes adjacent to the outer surfaces. Since identical penetration depths occur with other complexes, which differ from $Fe(CO)_5$ in both size and mechanism of adsorption,[14,41,42,54] the apparent penetration is taken as a measure of the deviations from surface planarity. It is not possible to determine the distribution of $Fe(CO)_5$(ads) on the powdered glass. Nevertheless, the rapid rate

(54) Strekas, T. C.; Gafney, H. D.; Goonatilake, H. W. *Inorg. Chem.* **1985**, *24*, 4439–41.

of desorption from these samples suggests that adsorption is also limited to the outer surfaces with the larger amount adsorbed, 3×10^{-4} moles/g, reflecting the larger outer surface area. Impregnation with $Fe_3(CO)_{12}$ is also limited to the outer surfaces, and with both monomer and trimer, UV–visible spectra recorded at different locations on the same sample establish a uniform adsorbate distribution on outer surfaces. The distribution of $Fe(CO)_5$(ads) as well as the sampling depth of the DRIFT technique, ca. 20–40 μm, limits the reactions examined in these experiments to $Fe(CO)_5$(ads) on the outermost surfaces of the support.

Lewis acid sites, principally B_2O_3, are present on the surface,[30,31] but no spectroscopic evidence was obtained in these experiments that suggests either preferential adsorption onto these sites or their involvement in the observed chemistry. Adsorptions of $Fe(CO)_5$ and $Fe_3(CO)_{12}$ are random processes that lead to uniform impregnations of the outer surfaces of the PVG sample.

With the exception of $Fe_2(CO)_9$, which disproportionates on the surface, adsorption of $Fe(CO)_5$ and $Fe_3(CO)_{12}$ occurs without chemical change. The electronic spectrum of the adsorbed trimer, a visible absorption at 605 nm, and an intense UV absorption with a shoulder at 440 nm closely resemble the fluid solution spectrum.[37] Its DRIFT spectrum, a major band at 2053 cm^{-1} with a broad shoulder at 2032 cm^{-1}, also closely resembles its fluid solution spectra.[38,39] Similarly, the electronic spectrum of $Fe(CO)_5$(ads), an increasing absorbance in the UV with a maximum at ≥230 nm and, although not well resolved after substraction of the intense absorptions due to PVG, ligand field bands at 252 and 285 nm, resembles the fluid solution spectrum of the complex. Lower energy ligand field transitions indicative of ligand substitution or visible absorptions indicative of dimeric and trimeric clusters are not detected. Relative to the gas-phase spectrum, where the band maxima occur at 2033 and 2012 cm^{-1}, DRIFT spectra of $Fe(CO)_5$(ads) (Figure 3) exhibit intense ν_{CO} bands at 2026 and 2004 cm^{-1} and a weak band at 2114 cm^{-1}. Jackson and Thrushiem report similar shifts when the complex is adsorbed onto silica gel.[18]

The weak band at 2114 cm^{-1} is assigned to the symmetric ν_1 mode since this mode occurs at 2117 cm^{-1} in the Raman spectrum of gaseous $Fe(CO)_5$.[44] Although forbidden under D_{3h} symmetry, a weak band at 2115 cm^{-1} does appear in the spectrum of crystalline $Fe(CO)_5$ where the molecular symmetry is C_2.[36] Its appearance in the $Fe(CO)_5$(ads) spectrum might be taken as evidence of adsorbate aggregation in the microscopic pore openings on the PVG surface. Aggregation is important in understanding cluster formation on a support and cannot be completely discounted. However, the absence of a significant increase in intensity with increasing loading, at least within the range of concentrations accessible to the DRIFT technique, suggests that the appearance of the 2115 cm^{-1} band arises not from aggregation on PVG but from molecular distortions that occur on adsorption. Bien and Jacobs report a weak ν_1 band at 2115 cm^{-1} when the complex is adsorbed onto different zeolites and attribute its occurrence to molecular distortions imposed by the support.[45] In spite of this apparent distortion, the similarity of the spectra of $Fe_3(CO)_{12}$(ads) and $Fe(CO)_5$(ads) with their respective solution spectra establishes that each complex adsorbs as a molecular entity without disruption of their primary coordination spheres. Therefore, changes in photochemical reactivity are not a consequence of molecular changes but rather a consequence of constraints imposed by the support.

The photochemistry of $Fe(CO)_5$(ads) initially parallels that found in fluid solution.[12] UV photolysis induces CO dissociation and the formation of a surface-confined photoproduct that adsorbs at 370 nm. The spectral change occurs with maintainance of an isosbestic point at 285 nm during the first few percent of reaction, and exposure to CO regenerates $Fe(CO)_5$(ads) in ≥97% yield. $Fe(CO)_4$ generated in low-temperature matrices exhibits absorptions at 340 nm and a band in the near-IR, whereas $Fe(CO)_4Q$, where Q represents occupation of vacant coordination site by matrix atom or molecule, exhibits only the 370-nm absorption.[46-48] Both species react with CO to regenerate $Fe(CO)_5$. The similarity of the product spectrum on PVG with that of $Fe(CO)_4Q$ establishes formation of the tetracarbonyl in which the vacated coordination site is occupied. Although surface silanol groups and/or chemisorbed water are capable of acting as weak ligands,[13,14] occupation does not necessarily imply formal coordination to the PVG surface. Recent measurements yield a $W(CO)_5$–PVG interaction energy of ≤7 kcal/mol,[14] which is considerably less than that expected for formal coordination to the surface. Clearly, the $Fe(CO)_4$–PVG interaction energy may differ, yet the interaction with the surface stabilizes the primary product, but not, as indicated by the facile, quantitative reaction with CO, at the expense of subsequent thermal or, as described below, photochemical reactivity.

Reaction 1, which characterizes the primary photoprocess, is independent of initial loading and occurs with a quantum yield, 0.96 ± 0.05. The latter is within experimental error of that in fluid solution, where the value is thought to be essentially unity.[12] The subsequent photochemistry, however, depends on the initial loading. With samples containing $\leq 10^{-6}$ mol of $Fe(CO)_5$/g, continued 254-nm photolysis leads to the evolution of 4.9 ± 0.2 mol of CO evolved/mol of $Fe(CO)_5$(ads). The absence of H_2 evolution[50,51] and the rapid reformation of $Fe(CO)_4$(ads) when the photoproduct is exposed to CO indicates that decarbonylation occurs without a concurrent oxidation of the iron atom. UV–visible spectra recorded during photolysis give no indication of formation of dimeric or trimeric clusters. Rather, in a number of experiments, a superimposed line spectrum after exhaustive 254-nm photolysis suggests that some of the complex decomposes to atomic iron.[52] Basset and co-workers report that Fe particles of ≤35-Å diameter, prepared by thermal decomposition of $Fe(CO)_5$ physisorbed onto silica gel, exhibit an FMR resonance with $g = 2.01$ and a line width of 2500 G at 25 °C.[53] The larger FMR line width of the photoproduct on PVG, $(5 \pm 0.5) \times 10^3$ G with $g = 2.070$ at 22 ± 1 °C, and the superimposed electronic line spectrum indicate the formation of smaller particles and in some cases atomic iron. Although the level of aggregation is not reproducible and varies from sample to sample, the photochemistry at low sample loadings, i.e., progressive decarbonylation without spectral evidence of dimer or trimer formation, is reproducible and differs from that observed on silica gel. The absence of trimer formation in these low loading experiments cannot be attributed to thermal instability or secondary photolysis. $Fe_3(CO)_{12}$(ads) is thermally stable at 25 °C in vacuo or under 1 atm of CO, and its quantum yield for decomposition, 0.07 ± 0.03 in vacuo, is small in comparison to those for reaction 1 and the monomeric photoproducts. Jackson and Thrusheim find that photolysis of $Fe(CO)_5$ on silica gel at room temperature leads to $Fe_3(CO)_{12}$ formation even at considerably less than monolayer coverage.[18] Since the surfaces of silica gel and PVG are similar,[29-31] this difference cannot be attributed to chemical factors. More likely, the difference reflects the dimensionalities of the surfaces. Recent measurements of the fractal dimension of PVG yields values ranging from 1.72 ± 0.12[32] to 2.5–2.6.[55] Although the uncertainity is large, the measured values are consistently smaller than those for silica gel, where $d = 2.94 \pm 0.06$.[28] We believe that the difference in the photochemistry of $Fe(CO)_5$ on these chemically similar surfaces arises from constraints imposed by the lower dimensionality PVG surface.

The photochemistry at higher loadings resembles that found on silica gel.[18] A 350-, 310-, or 254-nm photolysis of $Fe(CO)_5$(ads) at higher surface loadings, i.e., $\geq 10^{-6}$ mol/g, causes an immediate growth in absorbance at 605 nm. The product spectrum, which is equivalent to the visible spectrum of $Fe_3(CO)_{12}$(ads), establishes trimer formation. The stoichiometry of CO evolution (Figure 5) and the dependence of the quantum yield of trimer formation, ϕ_T, on irradiation time (Figure 6) indicate a complex reaction sequence. In addition to Fe_3CO_{12}(ads), a maximum at 370–380 nm in the photoproduct spectrum indicates the presence of the primary product $Fe(CO)_4$(ads).[46] Since CO scavenges the tetracarbonyl to reform $Fe(CO)_5$ and quenches trimer formation, the induction period in Figure 6 implies that trimer formation

(55) Drake, M., private communication, 1985.

arises from secondary reaction(s) of the primary photoproduct. Jackson and Thrusheim postulate that the primary photoproduct on silica gel, analogous to $Fe(CO)_4$(ads), undergoes a sequence of thermal reactions leading to $Fe_3(CO)_{12}$ formation.[18,25] Although not detected at room temperature, photolyses of $Fe(CO)_5$ on silica gel at temperatures between 10 and 50 K reveal a transient dimeric intermediate with bands in the bridging CO region at 1860 and 1820 cm^{-1}.[25] Since $Fe_2(CO)_9$ disproportionates on silica gel[18] and an increase in bands assigned to $Fe(CO)_5$ and $Fe_3(CO)_{12}$ accompanies the disappearance of bands assigned to the dimeric intermediate, trimerization on silica gel was attributed to a stepwise reaction sequence in which mobile $Fe(CO)_4$ thermally reacts with a surface-bound tetracarbonyl, designated $Fe(CO)_4$(OSi), to form a dinuclear intermediate that quickly reacts with $Fe(CO)_5$(ads) to form $Fe_3(CO)_{12}$(ads).[25]

Electronic spectra recorded during our experiments offer no indication of a shoulder in the 440-nm region that might be assigned to a dimeric intermediate. However, DRIFT spectra are consistent, in the general sense, with the stepwise reaction sequence proposed by Jackson and Thrushiem.[18,25] Spectra of the terminal CO region recorded after either pulsed 355-nm or continuous 350-nm photolysis of $Fe(CO)_5$(ads) on PVG under CO pressures ranging from 0.04 to 400 torr (Figures 7 and 10) reveal the immediate appearance of three bands at 2073, 2062, and 2048 cm^{-1}. The bands at 2073 and 2048 cm^{-1} appear first and, since the band intensities correlate well under different experimental conditions, are assigned to a single species. Continued photolysis leads to preferential formation of the species characterized by the 2062 cm^{-1} band. Both species rapidly react with CO at different rates to regenerate $Fe(CO)_5$(ads). However, neither species can be assigned to free $Fe(CO)_4$, which generally exhibits bands in 2000–1950 cm^{-1} region.[46-48,56] Rather, consistent with the electronic spectra that indicate occupation of the vacated coordination site, the relatively high-frequency CO bands closely resemble those of known oxidative addition products.[56-59] Sweany, for example, reports that UV photolysis of $Fe(CO)_5$ in an Ar matrix containing 10% H_2 yields $Fe(CO)_4$ that exhibits bands at 1994 and 1974 cm^{-1} and an oxidative addition product, $Fe(CO)_4H_2$, that exhibits bands at 2122, 2051, and 2043 cm^{-1}.[56] Ballivet-Tkatchenko and Coudurier assign bands that appear at 2112, 2040, 1985, and 1950 cm^{-1} when $Fe(CO)_5$ is adsorbed onto HY zeolites to a bound tetracarbonyl, designated ZOH-$Fe(CO)_4$.[8] Since the photoproduct spectra closely resemble those of known $Fe(CO)_4$ oxidative addition products,[56-59] the bands at 2072 and 2048 cm^{-1} are assigned to H-$Fe(CO)_4$-OSi where the primary photoproduct $Fe(CO)_4$ has undergone oxidative addition of a surface silanol group. Continued photolysis leads to preferential formation of the more reactive, 2062 cm^{-1} species. The latter is not a secondary photoproduct since formation of the 2062 cm^{-1} band does not occur with a concurrent decline in the 2072–2048 cm^{-1} bands of H-$Fe(CO)_4$-OSi. Since this band also appears in the region of known, monomeric, oxidative addition products but is more reactive than H-$Fe(CO)_4$-OSi, the 2062 cm^{-1} species is assigned to H-$Fe(CO)_4$-OH, where the primary photoproduct oxidatively adds chemisorbed water. Although calcination significantly reduces the water content of PVG, DRIFT spectra of the calcined samples indicate the presence of hydrogen-bonded water. It is not possible, since both H-$Fe(CO)_4$-OSi and H-$Fe(CO)_4$-OH are expected to exhibit similar electronic spectra, to unequivocally assign either to the 370-nm absorption. On the basis of the rapid decay of H-$Fe(CO)_4$-OH and the time required to record the electronic spectrum, however, most likely the 370-nm band is due principally to H-$Fe(CO)_4$-OSi.

In spite of their similarity, these are distinct, noninterconvertible photoproducts. H-$Fe(CO)_4$-OSi formation is essentially independent of CO pressure whereas H-$Fe(CO)_4$-OH formation is favored by higher CO pressure. Both species decay independently under CO to regenerate $Fe(CO)_5$(ads), and the more rapid decay of H-$Fe(CO)_4$-OH indicates that this is the more reactive product. Yet, the absence of a concurrent growth of the 2072–2048 cm^{-1} bands indicates that the H-$Fe(CO)_4$-OH decay pathway does not involve H-$Fe(CO)_4$-OSi formation. Although more stable, H-$Fe(CO)_4$-OSi is formed in limited amounts. This limited yield, in spite of an abundance of silanol groups on the PVG surface, is attributed to restrictions imposed by the low dimensionality of the PVG surface. Recent measurements in this laboratory, for example, indicate that the distortional freedom of a photoexcited adsorbate[60] as well as the surface mobility of $Fe(CO)_n$(ads) species are significantly curtailed at temperatures as high as 100 °C, on the PVG surface. Either restriction, i.e., the distortional freedom of the primary photoproduct or its surface mobility, curtails access to the silanol groups, and continued photolysis leads to preferential formation of H-$Fe(CO)_4$-OH. In contrast to H-$Fe(CO)_4$-OSi, which is formed immediately after excitation in both CO and CO-free experiments, H-$Fe(CO)_4$-OH formation is *not* detected in CO-free experiments. Rather, under these conditions, there is immediate spectral evidence of cluster formation. In addition, H-$Fe(CO)_4$-OH formation and cluster formation are both favored by longer excitation times. As stated above, however, H-$Fe(CO)_4$-OH is not a secondary photoproduct of H-$Fe(CO)_4$-OSi. Since the dependence of cluster formation on these reaction parameters correlates with the dependencies exhibited by H-$Fe(CO)_4$-OH, whereas H-$Fe(CO)_4$-OSi formation is relatively insensitive to the parameters, H-$Fe(CO)_4$-OH, rather than H-$Fe(CO)_4$-OSi, is the reactive precursor to cluster formation. Jackson and Thrushiem propose that a tetracarbonyl is the so-called "mobile intermediate" that reacts either thermally or photochemically to form the cluster products.[25] Although the above kinetic correlations point to H-$Fe(CO)_4$-OH as the precursor to cluster formation, the DRIFT spectra clearly establish that it does not per se thermally react to form a cluster. In fact, since the thermal decays of both oxidative addition products after photolysis occur without a concurrent increase in bands attributable to dimeric or trimeric clusters, neither surface-bound tetracarbonyl reacts thermally, at least on PVG, to form a cluster product. Additional photonic energy is required for cluster formation.

The induction period proceeding cluster formation (Figure 6) illustrates the conversion of the unreactive surface-bound tetracarbonyl to a more reactive intermediate. Steady-state photolyses of samples containing $\leq 10^{-6}$ mol of $Fe(CO)_5$(ads)/g establish a facile progressive decarbonylation, and TMP trapping experiments confirm the presence of $Fe(CO)_n$ ($n \leq 3$) species under conditions of cluster formation. Under 100 torr of TMP, CW photolysis (Figure 11) results in the immediate appearance of bands at 2047, 1969, 1940, and 1885 cm^{-1} that dominate the spectrum. On the basis of their close similarity to IR spectra of the corresponding triphenylphosphine complexes in hydrocarbon solution, the bands at 2047, 1969, and 1940 cm^{-1} are assigned to $Fe(CO)_4$(TMP) while the band at 1885 cm^{-1} is assigned to $Fe(CO)_3(TMP)_2$.[61] Continued photolysis leads to bands characteristic of dimeric species, and at the longest excitation times, 6.4 s, spectral substraction reveals bands at 1950, 1920, 1855, and 1815 cm^{-1}. The rapid decay of these bands after photolysis points to more highly unsaturated intermediates. The bands at 1950 and 1920 cm^{-1} are similar to those of $Fe(CO)_4$(TMP)[61] but, in view of their more rapid decay, are tentatively assigned to $Fe(CO)_3$(TMP). The bands at 1855 and 1815 cm^{-1} are tentatively assigned to $Fe(CO)_2(TMP)_2$ and $Fe(CO)_2(TMP)_3$, respectively. These are tentative assignments, but the appearance of bands, which can be assigned, based on their similarity to known spectra, to $Fe(CO)_3(TMP)_2$, even at the shortest irradiation times, establishes that laser excitation can induce either multiple CO loss and/or a facile photoinduced conversion of the primary product to a more coordinatively unsaturated species. Although multiple CO loss

(56) Sweany, R. L. *J. Am. Chem. Soc.* **1981**, *103*, 2410-2.
(57) Barraclough, C. C.; Lewis, J.; Nyholm, R. S. *J. Chem. Soc.* **1961**, 2582-4.
(58) Stobart, S. R. *J. Chem. Soc., Dalton Trans.* **1972**, 2442-7.
(59) Murdoch, H. D.; Weiss, E.; Lucken, E. A. C. *Helv. Chim. Acta* **1962**, *45*, 1927-33; **1964**, *47*, 1517-24.
(60) Shi, W.; Wolfgang, S.; Strekas, T. C.; Gafney, H. D. *J. Phys. Chem.* **1985**, *89*, 974-8.
(61) Graff, J. L.; Sanner, R. D.; Wrighton, M. S. *Organometallics* **1982**, *1*, 837-42.

has been established in vapor phase,[62] whether it occurs on this support is not established by our data. Nevertheless, the loss of the isosbestic point at 285 nm shortly after the onset of photolysis of $Fe(CO)_5$(ads) indicates a facile secondary photochemical reaction. Since the loss of the isosbestic point is not accompanied by pronounced increase in product absorbance, secondary photolysis of the surface-bound tetracarbonyl must occur with quantum efficiency similar to that for the conversion of $Fe(CO)_5$(ads) to $Fe(CO)_4$ oxidative addition products, i.e., close to unity.[63] The point is that photolysis quickly generates, in addition to the surface-bound tetracarbonyls, more highly unsaturated intermediates that satisfy criteria for the surface mobility essential to cluster formation at low surface coverages.

Unlike the tetracarbonyl that can bind to a single surface functionality, more highly unsaturated intermediates are unable to complete their coordination shell by binding to the surface. Studies of a variety of hydroxylated silicas indicate 4–7 silanol groups/100 Å^2.[64,65] With the assumption of an average of five Si–OH groups, symmetrically placed at the corners and the center of 10-Å square, the distances $Fe(CO)_3$ would have to span to complete its coordination shell exceed normal bond lengths. Consequently, either $Fe(CO)_n$ ($n \leq 3$) species on the surface are coordinatively unsaturated and/or the bonds to the surface are weak. Either possibility would promote surface mobility by the molecules exchanging from site to site trying to achieve complete coordination and a stable configuration. We believe that the drive to complete its coordination shell promotes mobility and that the more highly coordinatively unsaturated species are the mobile precursors to cluster formation. In fact, the large increase in the bands assigned to $Fe(CO)_3(TMP)_2$ and a corresponding increase in the bands assigned to the dimeric intermediate $Fe_2(CO)_8(TMP)$ (see below) specifically point to $Fe(CO)_3$ as the mobile precursor to dimer and most likely trimer formation.

Electronic spectra show that trimer formation declines as the CO pressure increases. The more rapid decay of the 2073 and 2048 cm^{-1} bands of H–$Fe(CO)_4$–OSi and the 2062 cm^{-1} band of H–$Fe(CO)_4$–OH under higher CO pressures indicates that CO scavenges these tetracarbonyls prior to cluster formation. The conspicuous absence of the 2062 cm^{-1} band of H–$Fe(CO)_4$–OH in DRIFT spectra that reveal clusterification led to the conclusion that H–$Fe(CO)_4$–OH rather than H–$Fe(CO)_4$–OSi is the principal precursor to cluster formation. This does not imply, however, since neither thermally reacts by itself to form a cluster, that H–$Fe(CO)_4$–OH rather than H–$Fe(CO)_4$–OSi undergoes secondary photolysis. The similarity of their electronic spectra makes preferential excitation of one in the presence of the other, particularly when both are present on the outer surface of the support, very unlikely. Most likely both undergo secondary photolysis, although some difference in quantum efficiency might be expected in view of the differences in their thermal decays. Since H–$Fe(CO)_4$–OSi is formed in limited amounts whereas continuous photolysis leads to preferential formation of H–$Fe(CO)_4$–OH, the latter is the dominant tetracarbonyl on PVG. Being more reactive and in the largest amount, its absence during clusterification suggests that H–$Fe(CO)_4$–OH rather than H–$Fe(CO)_4$–OSi is the tetracarbonyl that reacts with the more highly unsaturated, mobile intermediates to form the dimeric and trimeric clusters. However, this does not represent the sole clusterification pathway. Although the photon flux during laser excitation is sufficient to photolyze the majority of $Fe(CO)_5$(ads) in the exposed area, the rapid reappearance of pentacarbonyl due to either recombination with the photoejected CO or diffusion of unreacted $Fe(CO)_5$(ads) into the photolyzed region establishes its presence in the reaction region. The initial substraction of the $Fe(CO)_5$ spectrum precludes detection of this reaction pathway, but analogy to the photoinduced dimerization of the complex in noncoordinating solvents[19-22] suggests that $Fe(CO)_5$ may also be involved in clusterification.

Scheme I

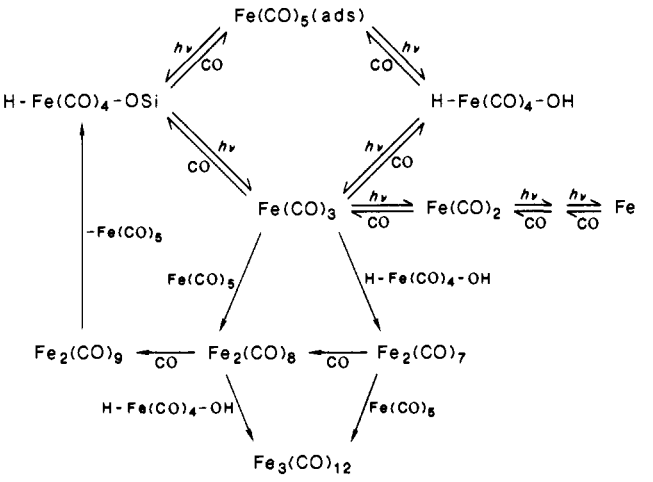

The band at 2053 cm^{-1} (Figure 9) agrees with the major band of $Fe_3(CO)_{12}$ sublimed onto PVG and is assigned to the trimer. $Fe_3(CO)_{12}$(ads) is stable, and its spectrum does not change after photolysis. In addition to $Fe_3(CO)_{12}$(ads), DRIFT spectra recorded following pulsed excitation of $Fe(CO)_5$(ads) in vacuo (Figure 7) exhibit weaker bands at 2056, 2068 and 1790, and 2066 and 1820 cm^{-1}. Unlike the 2053 cm^{-1} band of $Fe_3(CO)_{12}$(ads), the 2056 cm^{-1} band decays after photolysis. Since it occurs in the trimer region, although at slightly higher frequency, it is assigned to an incompletely formed trimer, $Fe_3(CO)_n$(ads) ($n \leq 11$), in which the vacant coordination sites are most likely occupied by a surface functionality. The weak bands at 2068 and 1790 cm^{-1} and 2066 and 1820 cm^{-1} (Figure 9) closely resemble those in low-temperature matrices described by Poliakoff and Turner[52] and are assigned to $Fe_2(CO)_8$ and $Fe_2(CO)_9$, respectively. Consistent with the reactivity of $Fe_2(CO)_8$ and the disproportionation of $Fe_2(CO)_9$ on silica gel[18] or PVG at room temperature, both dimeric intermediates decay rapidly after photolysis. Since the decay of H–$Fe(CO)_4$–OSi following CW excitation is detectable only after the decay of the dimeric intermediates $Fe_2(CO)_9$ and $Fe_2(CO)_8$ decay to $Fe(CO)_5$ via H–$Fe(CO)_4$–OSi.

In addition to bands assigned to monomeric substitution products, TMP trapping yields additional evidence of dimeric intermediates. Spectra recorded after CW photolysis under 100 torr of TMP (Figure 11) reveal bands at 2020, 2004, 1998, and 1845 cm^{-1}, which are tentatively assigned to the monosubstituted phosphine analogue of $Fe_2(CO)_9$, $Fe_2(CO)_8(TMP)$. Monosubstituted, dimeric complexes have not been isolated in solution. However, the decay of each is consistent with the disproportionation of a dimer into $Fe(CO)_4L$ and $Fe(CO)_5$. The decay of the bands attributed to $Fe_2(CO)_8(TMP)$, for example, occurs with a concurrent increase in the bands assigned to $Fe(CO)_4(TMP)$. Continued photolysis yields a band at 1788 cm^{-1} that, being in the bridging carbonyl region, is tentively assigned to $Fe_2(CO)_7(TMP)_2$.

A summary of the intermediates and their interconversions on PVG is presented in Scheme I. Although written in terms of sequential photoinduced decarbonylation steps, our data do not preclude, particularly with laser excitation, multiple CO loss. In either case, however, the result is the same since steady-state photolyses indicate that secondary photolysis occurs with a relatively high quantum efficiency.[46,47,52,66-68] In a general sense, the reaction mechanism agrees with the mechanism postulated by Jackson and Thrushiem.[18,25] However, there are a number of obvious differences. Bands in the 1960–1940 cm^{-1} region, which have been assigned by several investigators to $Fe(CO)_4(SiO_2)$,[8,25,45,46,48] are not observed on PVG. Rather, UV photolysis

(62) Nathanson, G.; Gitlin, B.; Rosan, A. M.; Yardley, J. T. *J. Chem. Phys.* **1972**, *74*, 361–9, 370–8.
(63) Von Gustorf, K.; Grevels, E. F. *Top. Curr. Chem.* **1969**, *13*, 366–450.
(64) Synder, L. R.; Ward, J. W. *J. Phys. Chem.* **1966**, *70*, 3941–52.
(65) Reference 29, pp 622–714.
(66) Poliakoff, M. *Chem. Soc. Rev.* **1978**, *7*, 527–40.
(67) Ouderkirk, A. J.; Wermer, P.; Shultz, N. L.; Weitz, E. *J. Am. Chem. Soc.* **1983**, *105*, 3354–5.
(68) Ouderkirk, A. J.; Weitz, E. *J. Chem. Phys.* **1983**, *79*, 1089–91.

of $Fe(CO)_5$ physisorbed onto PVG leads to the immediate formation of two species that are assigned, based on their spectral similarity to known oxidative addition products,[56-59] to H–Fe(CO)$_4$–OSi and H–Fe(CO)$_4$–OH. The latter species is more reactive and is the tetracarbonyl that reacts with more highly unsaturated intermediates, principally $Fe(CO)_3$, to form cluster products. These oxidative addition species are short-lived at room temperature and may not be detectable with a dispersive spectrophotometer. In the low-temperature experiments performed by Jackson and Thrushiem,[25] where $Fe(CO)_4(SiO_2)$ is detected, a band at 2060 is assigned to $Fe_3(CO)_{12}$. Since the lifetimes of H–Fe(CO)$_4$–OSi and H–Fe(CO)$_4$–OH would be expected to be longer at low temperatures, it is possible that this band comprises absorptions due to these oxidative addition products, whereas at room temperature $Fe_3(CO)_{12}$ may indeed be the sole contributor to the band.

The second difference is that, unlike photolysis of $Fe(CO)_5$ physisorbed onto silica gel where $Fe_3(CO)_{12}$ formation occurs at considerably less than monolayer coverage,[18] electronic spectra recorded during 254-, 310-, or 350-nm photolysis of PVG samples containing $\leq 10^{-6}$ mol of $Fe(CO)_5$(ads)/g, causes progressive decarbonylation with no indication of trimer formation. In view of the chemical similarity of the silica gel and PVG surfaces,[29-31] it is tempting to attribute the differences in the observed reactivity to the reported differences in the fractal dimensionalities of the surfaces.[28,32,55] However, additional data regarding the photochemical reactivity of adsorbates on chemically similar surfaces of different dimensionalities are needed to resolve the role of surface dimensionality. In our opinion, the dimensionality of the PVG surface most likely plays a role in curtailing adsorbate mobility, but it is not the sole factor controlling this observed difference in the dependence of trimer formation, or clusterification in general, on the initial amount of $Fe(CO)_5$ adsorbed. Rather, the difference in the chemistry may arise from differences in the methods of excitation. In those experiments where conventional, low-power density light sources, such as a Rayonet reactor, were used, there is no evidence, regardless of the initial loading, of desorption of $Fe(CO)_5$. On the other hand, laser excitation, even at the lowest power densities, causes an immediate, essentially complete loss of the $Fe(CO)_5$(ads) spectrum. Since the $Fe(CO)_5$(ads) spectrum quickly redevelops without a concurrent change in the photoproduct spectrum, laser excitation, because of its high-power density and potential heating of the adsorbent surface, apparently causes significant desorption of the complex. Considering the volitility of $Fe(CO)_5$ and its weak physisorption onto these surfaces, if desorption is rapid in comparison to the pulse duration, particularly with a highly scattering support, significant photochemistry could be occurring in the vapor phase, where the longer lifetimes of various intermediates would promote cluster formation and, due to the higher molecular weight and lower volatility of the resulting cluster, readsorption of the cluster onto the surface.

Conclusions

$Fe(CO)_5$ physisorbs onto PVG without disruption of its primary coordination sphere. UV photolysis of the adsorbed complex leads to efficient formation of a tetracarbonyl that rapidly reacts with the PVG surface to form H–Fe(CO)$_4$–OSi and H–Fe(CO)$_4$–OH. Depending on the initial loading, continued photolysis leads to further decarbonylation and formation of, in some cases, atomic iron or elemental iron aggregates. With samples containing $\geq 10^{-6}$ mol of $Fe(CO)_5$(ads)/g, UV photolysis leads to $Fe_3(CO)_{12}$(ads) formation. Cluster formation occurs by a photochemically driven, stepwise reaction sequence in which the so-called "mobile intermediate", principally $Fe(CO)_3$, reacts with H–Fe(CO)$_4$–OH or $Fe(CO)_5$(ads) to form dimeric intermediates that either decay to H–Fe(CO)$_4$–OSi or react in subsequent steps to form the stable product $Fe_3(CO)_{12}$(ads).

Acknowledgment. Support of this research by the Research Foundation of the City University of New York, the Dow Chemical Company's Technology Acquisition Program, and the National Science Foundation (CHE-8511727) is gratefully acknowledged. M.S.D. thanks the Dow Chemical Co. for a Graduate Research Associateship at the Dow Laser Laboratory. H.D.G. thanks the Andrew W. Mellon Foundation for a fellowship during 1983–1984 and the Corning Glass Works for samples of porous Vycor glass.